Domain walls and Dzyaloshinskii-Moriya interaction in epitaxial Co/Ir(111) and Pt/Co/Ir(111)

Marco Perini,[1,*] Sebastian Meyer,[2] Bertrand Dupé,[2,†] Stephan von Malottki,[2] André Kubetzka,[1] Kirsten von Bergmann,[1] Roland Wiesendanger,[1] and Stefan Heinze[2]

[1]*Department of Physics, University of Hamburg, Jungiusstrasse 11, D-20355 Hamburg, Germany*
[2]*Institute of Theoretical Physics and Astrophysics, Christian-Albrechts-Universität zu Kiel, Leibnizstrasse 15, D-24098 Kiel, Germany*

We use spin-polarized scanning tunneling microscopy and density functional theory (DFT) to study domain walls (DWs) and the Dzyaloshinskii-Moriya interaction (DMI) in epitaxial films of Co/Ir(111) and Pt/Co/Ir(111). Our measurements reveal DWs with fixed rotational sense for one monolayer of Co on Ir, with a wall width around 2.7 nm. With Pt islands on top, we observe that the DWs occur mostly in the uncovered Co/Ir areas, suggesting that the wall energy density is higher in Pt/Co/Ir(111). From DFT we find an interfacial DMI that stabilizes Néel-type DWs with clockwise rotational sense. The calculated DW widths are in good agreement with the experimental observations. The calculated total DMI nearly doubles from Co/Ir(111) to Pt/Co/Ir(111); however, in the latter case the DMI is almost entirely due to the Pt with only a minor Ir contribution. Therefore a simple additive effect, in which both interfaces contribute significantly to the total DMI, is not observed for one atomic Co layer sandwiched between Ir and Pt.

I. INTRODUCTION

In the field of spintronics, localized noncollinear magnetic structures such as domain walls (DWs) and skyrmions are promising candidates for innovative technological applications [1,2]. A key aspect in this field of research is the right choice of materials which can form such magnetic structures. Recently, cobalt-based multilayer systems have received significant attention due to the observation of magnetic skyrmions at room temperature [3–6]. The stabilization of these noncollinear magnetic states requires the competition of different interactions [3–9]. In particular, the interfacial Dzyaloshinskii-Moriya interaction (DMI) [10–13] favors magnetic structures with fixed rotational sense, such as Néel-type DWs [14,15] and skyrmions [7–9,16]. It occurs in systems with large spin-orbit coupling (SOC) and broken inversion symmetry, e.g., at the interfaces of cobalt and heavy materials possessing large SOC, such as iridium or platinum [17]. The DMI is extremely sensitive to the interface quality [18]. Sputtered films on amorphous or polycrystalline substrates, such as those studied in Refs. [3–5], are not well suited for a microscopic understanding of the details of the DMI since the interface roughness of such films is difficult to characterize experimentally and hard to include in first-principles calculations. *Ab initio* methods such as density functional theory (DFT) are crucial for an understanding of the DMI in multilayered systems [19], where multiple interfaces contribute to the total DMI and the effects of each one are hard to disentangle experimentally.

Epitaxially grown ultrathin films on single-crystal substrates are best suited for a detailed study of interface DMI.

These model-type systems can also be compared to first-principles calculations, enabling a disentanglement of the relevant interactions involved in the formation of magnetic states. Previous works have reported opposite signs of DMI at the Co/Ir and Co/Pt interfaces [20–22] and predicted an enhancement of the total DMI when the Co is sandwiched between the two heavy metals in a multilayer configuration, an effect often referred to as additive DMI [3,23]. This effect is not always observed in experiments with epitaxial films, as shown in Ref. [24] for Co/Ir/Ni multilayers. This suggests that the proposed mechanism of additive DMI still requires a deeper understanding. Magnetic DWs have been used in different materials to determine the sign of the interfacial DMI [24–27]. For DWs with a width in the single-digit nanometer range, spin-polarized scanning tunneling microscopy (SP-STM) has the necessary spatial resolution to image them. A previous SP-STM study on Co/Ir(111) showed that isolated Co monolayer (ML) islands on Ir are ferromagnetic in the out-of-plane direction, with large coercive fields H_c [28]. Such islands grow pseudomorphically on the Ir substrate, making Co/Ir(111) an optimal model system to study the properties of the interfacial DMI both experimentally and theoretically.

Here, we study pseudomorphic films of a Co ML and an atomic bilayer (BL) of Pt/Co on an Ir(111) surface. Using SP-STM we observe that the films exhibit out-of-plane magnetic domains, separated by nanometer-wide DWs. The DW widths are in very good agreement with those calculated from DFT parameters. We demonstrate experimentally that the DWs have a unique rotational sense. DFT calculations reveal that the DMI is almost twice as large in Pt/Co/Ir(111) as in Co/Ir(111). Surprisingly, the DMI in Pt/Co/Ir(111) is dominated by Pt, while the Ir contribution is nearly quenched compared to the bare Co/Ir(111) system. Thus an additive DMI effect as suggested in Ref. [3], where both interfaces have a significant contribution to the total DMI, is not observed in this case since

---

*mperini@physnet.uni-hamburg.de

†Present address: Institute of Physics, Johannes Gutenberg Universität Mainz, Staudingerweg 7, D-55128 Mainz, Germany.

TABLE I. Energy difference ΔE (meV/Co atom) between fcc and hcp stackings of the Pt top layer and interlayer distances d_{ij} (Å) after the structural relaxation of the film systems for the topmost layers. Note that for Co/Ir(111) the third and fourth layers are kept fixed and $d_{34} = d_{45} = d_{bulk}$ [for Pt/Co/Ir(111) $d_{45} = d_{bulk}$]. Layers without a subscript have fcc stacking.

System	ΔE	d_{12}	d_{23}	d_{34}	d_{45}	d_{bulk}
Co/Ir(111)		2.23	2.31			2.21
Pt/Co/Ir(111)	0	2.16	2.10	2.30		2.21
Pt$_{hcp}$/Co/Ir(111)	+21.0	2.16	2.10	2.31		2.21
Pt/Co/Co/Ir(111)		2.17	1.93	2.14	2.30	2.21
Pt/Pt/Co/Ir(111)		2.51	2.14	2.11	2.30	2.21

most of the DMI comes from only one interface. For a sandwich structure with a Co double layer, on the other hand, the DMI further increases, and both Pt and Ir contribute significantly, suggesting that in thicker multilayers the DMI indeed becomes larger because of an additive effect.

II. METHODS

A. Experimental details

The measurements were performed in ultrahigh vacuum (UHV) conditions using two low-temperature STM setups with base temperatures of 8 K [29] and 4.7 K [30]. To obtain spin resolution we use Cr bulk tips which have been prepared by chemical etching. The Ir(111) single crystals are prepared by cycles of Ar-ion sputtering at 800 eV, followed by annealing at temperatures of 1300 °C. The Co is then deposited onto the clean substrate held at temperatures around 100 °C, with deposition rates between 0.15 and 0.25 atomic layers per minute. The Pt is deposited on top of the Co with the substrate at room temperature.

B. Computational details

We used the full-potential linearized augmented plane wave method [31,32] in film geometry [33] as implemented in the FLEUR code [34]. For all our calculations, we chose the equilibrium lattice parameters of bulk Ir, i.e., 7.22 a.u., relaxed within the local-density approximation (LDA) [35]. Muffin-tin radii of 2.31 a.u. are chosen for Ir and Pt, and 2.26 a.u. is applied for Co. The energy cutoff for the basis functions was set to $k_{max} = 4.0$ a.u.$^{-1}$.

The structural relaxation was performed in the ferromagnetic (FM) state with a symmetric film consisting of five layers of Ir with a Co ML or a Pt/Co BL on both sides using the generalized gradient approximation ([36]) of the exchange-correlation (xc) functional. We minimized the forces between the uppermost layers in the [111] direction until they were smaller than 10^{-5} hartrees/a.u. while three layers of Ir were kept fixed. For Co/Ir(111) [Pt/Co/Ir(111), Pt/Co/Co/Ir(111), Pt/Pt/Co/Ir(111)] 110 (240) k points in the irreducible wedge of the Brillouin zone (BZ) were used. If not specified explicitly, all considered layers are in fcc stacking. The equilibrium interlayer distances for the different systems are presented in Table I. For Pt/Co/Ir(111) the energy difference is shown for the two stackings of Pt (fcc and hcp). Since Pt$_{fcc}$/Co/Ir(111) is
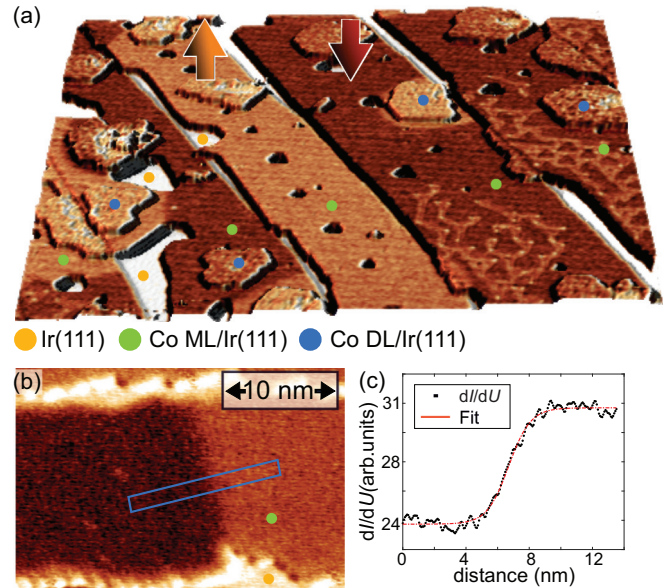

$\bullet$ Ir(111) $\bullet$ Co ML/Ir(111) $\bullet$ Co DL/Ir(111)

FIG. 1. (a) Perspective view of the topography of about 1.2 atomic layers of Co on Ir(111) (200 × 180 nm²), colorized with the simultaneously measured spin-resolved dI/dU signal. The arrows indicate two oppositely magnetized domains of the out-of-plane ferromagnetic Co ML stripes. The colored dots identify the different areas of Ir and Co ML and double layer (DL). (b) Closer view of a single DW. The signal inside the blue box is averaged in the short direction and then plotted against the long direction in (c). The red line is a fit of Eq. (1) to the data points, in arbitrary units. In (a) $U = -580$ mV, $I = 500$ pA, $T = 8$ K; in (b) $U = -450$ mV, $I = 500$ pA, $T = 8$ K.

favorable by about 21 meV/Co atom, we restrict ourselves to the fcc stacking of Pt.

We calculated the energy dispersion $E(\mathbf{q})$ of homogeneous, flat spin spirals [37,38] along the high-symmetry directions, $\overline{\Gamma}$-$\overline{M}$ and $\overline{\Gamma}$-$\overline{K}$, of the two-dimensional BZ. Spin spirals are characterized by the vector $\mathbf{q}$, which determines the propagation direction and the angle between two adjacent magnetic moments. In general, the magnetic moment of atom i is described by $\mathbf{M}_i = M[\cos(\mathbf{q} \cdot \mathbf{R}_i)\sin\theta, \sin(\mathbf{q} \cdot \mathbf{R}_i)\sin\theta, \cos\theta]$, where $\mathbf{R}_i$ is the position of atom i. In our case of flat spin spirals, we consider $\theta = 90°$. Without SOC, the generalized Bloch theorem is used to self-consistently calculate the spin spiral states in the chemical unit cell [37,39].

We use asymmetric films with a substrate of nine layers and the Co ML (Pt/Co BL) on one side. The distances between the topmost layers are set according to the structural relaxations from Table I. The vector $\mathbf{q}$ is chosen along the high-symmetry lines of the two-dimensional BZ. High-symmetry points are related to specific magnetic states: $\overline{\Gamma}$, the ferromagnetic (FM) state, $\overline{M}$, the row-wise antiferromagnetic (AFM) state, and $\overline{K}$, the Néel state.

For the calculation of the spin spiral states, we use a dense k-point mesh of 44 × 44 k points in the full BZ. Our energy cutoff is set to $k_{max} = 4.0$ a.u.$^{-1}$, and we applied the LDA [35] of the xc potential. The energy contribution due to SOC ΔE_{SOC} was calculated in first-order perturbation theory for every $\mathbf{q}$ point [38,40,41]. To evaluate the strength of the Heisenberg exchange and the DMI, we restrict ourselves to the region
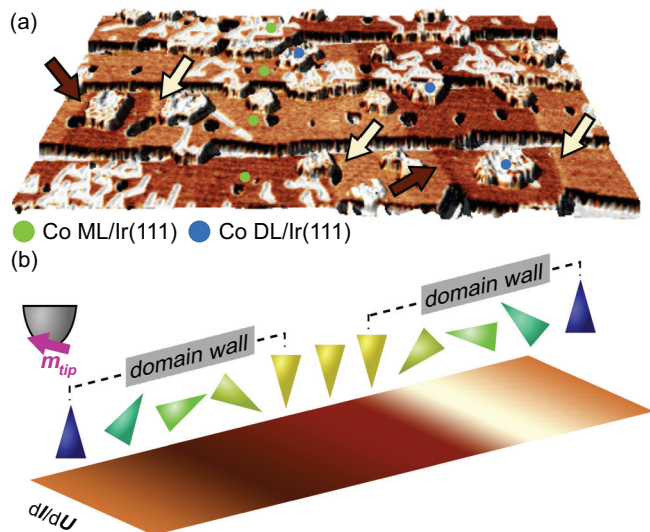
Co ML/Ir(111)   Co DL/Ir(111)

FIG. 2. (a) Perspective view of the topography of about 1.2 atomic layers of Co on Ir(111) (280×210 nm^2) colorized with the simultaneously measured spin-resolved dI/dU signal. The tip has a canted magnetization; that is, it is sensitive to both in-plane and out-of-plane magnetization components. The arrows indicate the position of the DWs and are colorized according to the dI/dU contrast of the walls. Neighboring walls in a stripe always show an alternating contrast. The colored dots identify the different areas of Co ML and DL. (b) Schematics of spin-resolved dI/dU contrast across two consecutive DWs with a tip that has canted magnetization. In (a) $U = -450$ mV, $I = 500$ pA, $T = 8$ K.

around the $\overline{\Gamma}$ point and use an effective nearest-neighbor approximation for both interactions, which are expressed by the parameters J and D, respectively. We have also performed a fitting of the spin spiral energy dispersions with exchange constants and DMI beyond nearest neighbors. Using these parameters within atomistic spin dynamics simulations leads to DW widths and energies which are not significantly different from those obtained based on the effective nearest-neighbor approximation. This approximation is therefore sufficient to describe accurately the DW properties in this system.

The magnetocrystalline anisotropy energy (MAE) was determined by calculating the energy difference K between the FM state with a magnetization direction pointing perpendicular to the film plane $E_\perp$ and the FM state with a magnetization in the film plane $E_\parallel$. We self-consistently calculated the FM state in scalar-relativistic approximation and applied the force theorem [42,43] for calculations with SOC.

III. RESULTS

A. Experimental results

A typical sample of Co grown on the Ir(111) substrate is shown in Fig. 1(a), in which the topography is colorized with the measured spin-polarized differential tunneling conductance (dI/dU), obtained using a magnetic tip sensitive to the out-of-plane component of the sample magnetization. Despite the 8% lattice mismatch, the Co ML mainly grows pseudomorphically with occasional dislocation lines to reduce the strain. Due to the smooth step flow growth we assume that
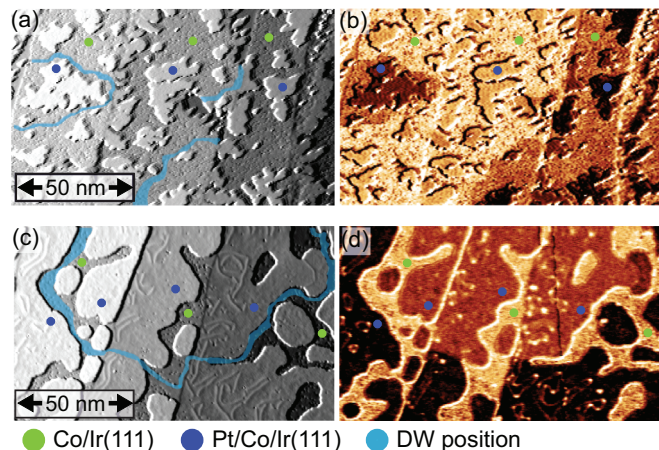

Co/Ir(111)   Pt/Co/Ir(111)   DW position

FIG. 3. (a) and (c) Constant-current topography maps of Pt/Co/Ir(111) in the as-grown case and after postannealing, respectively. The differentiated topography signal is superimposed on the maps to enhance the visibility of the topographic details. (b) and (d) Corresponding dI/dU maps measured with out-of-plane magnetic sensitivity. The blue lines trace the position of the DWs, which avoid Pt/Co when possible. The thickness of the lines accounts for the uncertainty of the exact position of the wall. In (a) and (b) $U = -450$ mV, $I = 1$ nA, $T = 8$ K; in (c) and (d) $U = -550$ mV, $I = 1$ nA, $T = 8$ K.

the Co is fcc stacked. The two levels of contrast on the Co indicate areas with a magnetization pointing in opposite out-of-plane directions [28] [see sketched arrows in Fig. 1(a)].

Figure 1(b) shows the dI/dU map of a Co ML stripe with a DW that separates oppositely magnetized out-of-plane domains. The dI/dU signal within the blue rectangle is plotted in Fig. 1(c) as a function of the position across the wall. The DW profile is fitted according to

$$y = y_0 + y_{sp}\tanh\left(\frac{x - x_0}{w/2}\right), \tag{1}$$

where y_0 and y_{sp} are the spin-averaged and spin-polarized contributions to the dI/dU signals, respectively, x_0 is the center of the DW, and w is the wall width. We fitted eight walls from different samples, obtaining an average of $w = (2.7 \pm 0.3)$ nm, where the uncertainty represents the standard deviation of the values.

Whereas in Fig. 1(a) the tip is dominantly sensitive to the out-of-plane magnetization of the domains, Fig. 2(a) shows a measurement where the magnetic DWs also have a contribution to the spin-resolved signal; that is, the tip magnetization is canted in this case. With such a tip the DWs appear as bright or dark stripes depending on the magnetization direction within the walls. We find a correlation of the magnetization within a wall with the order of the out-of-plane orientation of the domains it separates, as indicated by the differently colored arrows in Fig. 2(a). This strict sequence of spin-resolved dI/dU contrasts demonstrates that the DWs in the Co ML on Ir(111) have a unique rotational sense, as sketched in Fig. 2(b). This is confirmed by investigating 13 independent DWs with the same magnetic tip (not shown). We conclude that the interfacial DMI is large enough to select a unique rotational sense and propose that it also induces Néel-type

TABLE II. Calculated values for the effective nearest-neighbor exchange interaction J (meV), Dzyaloshinskii-Moriya interaction D (meV), magnetocrystalline anisotropy energy K (meV), calculated energy difference [14] $\Delta E_{\text{DW-FM}} = \frac{4}{a}\sqrt{2|JK|} - \frac{2}{a}\pi\sqrt{3}|D|$ between a DW and the FM state (meV/nm), and calculated DW width $w = 2a\sqrt{\frac{3J}{2|K|}}$, with a being the lattice constant of the (111) plane of the substrate, compared to the experimental DW width w_{exp} (nm). $D < 0$ represents clockwise rotation, and $K < 0$ represents an out-of-plane easy magnetization axis. All magnetic interactions are given per Co atom.

System	J	D	K	$\Delta E_{\text{DW-FM}}$	w	w_{exp}
Co/Ir(111)	+17.6	−0.54	−0.73	+53.3	3.2	2.7 ± 0.3
Pt/Co/Ir(111)	+18.0	−1.12	−1.00	+43.8	2.8	2.7,3.6
Pt/Pt/Co/Ir(111)	+22.5	−1.33	−0.83	+36.9	3.4	
Pt/Co/Co/Ir(111)	+20.0	−0.80	−0.09	−4.1	9.9	

DWs according to the symmetry selection rules [14,15,44]. An attempt to measure the absolute rotational sense of the DWs is presented in Appendix A.

To investigate the effect on the DWs when the Co is sandwiched between Pt and Ir, we performed additional measurements on Pt ML islands on top of an almost complete ML of Co on Ir(111). Figure 3(a) shows pseudomorphic Pt islands with irregular shapes grown with the Co/Ir(111) held at room temperature. The spin-resolved dI/dU contrast of the Pt islands in Fig. 3(b) is strongly correlated with that of the surrounding Co ML, and we conclude that the Co induces a magnetic polarization in the Pt and that the Pt/Co BL is also out of plane ferromagnetic. A closer look at the data in Fig. 3(b) reveals two slightly different dI/dU contrast levels for each

magnetization direction, originating from islands grown in the two different stackings.

In order to obtain more extended films of Pt, we postannealed such samples at moderate temperature ($T \simeq 500\,^\circ\text{C}$) after the Pt deposition. This results in a mostly fcc stacked Pt layer attached to the step edges, as shown in Fig. 3(c). The Pt layer still shows out-of-plane magnetization, induced by the Co ML [see Fig. 3(d)]. We can exclude the possibility of a significant degree of intermixing between Co and Pt since the electronic properties of each of the different materials, i.e., the dI/dU spectra of the Co ML and the Pt/Co BL, are found to be very similar in all samples. The blue lines in Figs. 3(a) and 3(c) mark the DWs, and the linewidth represents the uncertainty of their position. A close analysis demonstrates that the DWs tend to avoid the Pt/Co layer if possible, increasing their length in order to remain on the bare Co. This suggests a higher DW energy density in the Pt/Co BL compared to that of the Co ML on Ir(111). The DWs in the Pt/Co layer have the tendency to sit in very small constrictions. To minimize the effect of the constriction size on the DW width [45], we have selected walls occurring in areas at least twice as large as w, obtaining the values of 2.7 and 3.6 nm, similar to the ones in Co/Ir(111).

B. First-principles calculations

Figures 4(a) and 4(b) show the calculated energy dispersion for Co/Ir(111) in the $\overline{\Gamma}$-$\overline{K}$ and $\overline{\Gamma}$-$\overline{M}$ directions, respectively. The FM state is the lowest in energy, and the nearest-neighbor exchange interaction J (Table II) describes very well the energy dispersion. $\Delta E_{\text{SOC}}(\mathbf{q})$ is small compared to the variation of the exchange $E(\mathbf{q})$ (see D in Table II). The interfacial DMI results from the sum of the individual contributions from the different layers [see Figs. 4(c) and 4(d)], and it prefers
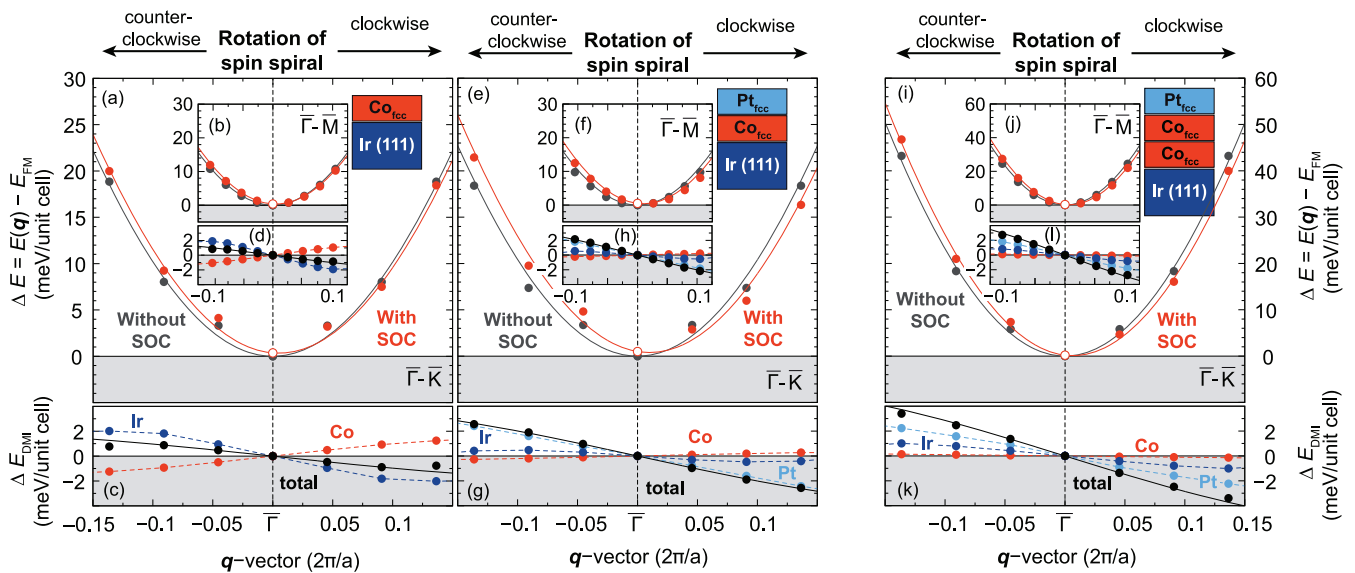

FIG. 4. (a) and (b) Calculated energy dispersion $E(\mathbf{q})$ of flat, cycloidal spin spirals for Co/Ir(111) without (gray dots) and with (red dots) spin-orbit interaction for left- and right-rotating spin spiral states in the $\overline{\Gamma}$-$\overline{K}$ and $\overline{\Gamma}$-$\overline{M}$ directions, respectively. The gray line is a fit of the dispersion to the Heisenberg model; the red line is a fit including the DMI and the magnetocrystalline anisotropy. (e) and (f) The same as (a) and (b), but for Pt/Co/Ir(111); (i) and (j) the same as (a) and (b), but for Pt/Co/Co/Ir(111). (c), (d), (g), (h), (k), and (l) Element-resolved energy contribution for Co/Ir(111), Pt/Co/Ir(111), and Pt/Co/Co/Ir(111) to the DMI $\Delta E_{\text{DMI}}(\mathbf{q})$. Note that the total DMI is the sum of all contributions and that all energies are given per unit cell [i.e., two magnetic atoms for Pt/Co/Co/Ir(111)]. The black curve is the fit of the DMI. All fits are made within an effective nearest-neighbor approximation.
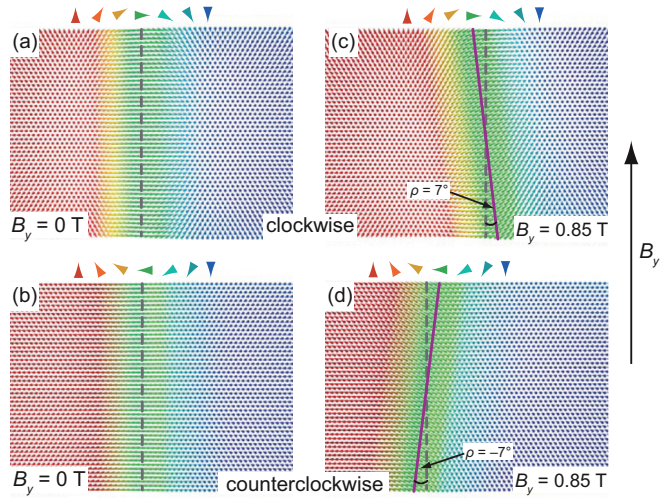
FIG. 5. Spin dynamics simulation with open-boundary conditions of two Néel DWs with opposite rotational sense; see side view sketches at the top of each panel. (a) and (b) DWs in zero field. (c) and (d) When an in-plane field B_y of 0.85 T is applied, the two walls tilt in opposite directions with an angle of about $\pm 7°$ to partially maintain their cycloidal configuration. The simulation is done with 150×50 spins and the exchange, DMI, and MAE values of Table II.

clockwise-rotating spin spirals ($D < 0$). The Ir surface dominates the total DMI; however, Co has a significant contribution of opposite sign, which we attribute to its small coordination number [41]. The MAE prefers an out-of-plane magnetization ($K_{eff} = -0.7$ meV; see Table II) that favors collinear states over spin spirals.

An atomic Pt overlayer does not modify the exchange interaction significantly with respect to Co/Ir(111) [see Figs. 4(e) and 4(f) and Table II]. In contrast, the MAE increases by about 50%, and the total DMI is more than two times larger. However, Figs. 4(g) and 4(h) show that such an increase in DMI is mostly due to the contribution from the Pt overlayer. The Ir substrate, on the other hand, has a minor contribution which is nearly quenched compared to its value in Co/Ir(111) [see Fig. 4(c)].

Adding another Pt adlayer does not change significantly the total DMI or the contributions from the two interfaces (see Appendix B). We conclude that the hybridization of the Co layer with both Ir and Pt has a decisive impact on the resulting DMI. A simple additive effect as suggested in Ref. [3], where the Pt/Co and Co/Ir interfaces contribute with a similar DMI strength in a Pt/Co/Ir multilayer, does not apply for one atomic Co layer. In order to gain further insight into this effect, we have performed calculations with an additional Co layer, i.e., Pt/Co/Co/Ir(111) [see Figs. 4(i)–4(l)]. While the exchange rises by about 10% per Co atom, the MAE is reduced by a factor of 10 compared to Pt/Co/Ir(111) (see Table II). The total DMI increases compared to the Pt/Co/Ir(111) system because of an enhanced Ir contribution, whereas the Pt contribution is similar to the one in Pt/Co/Ir(111). Thus for a Co double layer both the Pt/Co and Co/Ir interfaces, which are farther apart from each other, contribute significantly to the total DMI, supporting the interpretation of Ref. [3] of an additive DMI effect for this particular case. Note that the value of D given in Table II for Pt/Co/Co/Ir(111) is still smaller than for Pt/Co/Ir(111) since it is given per Co atom. The DW width and energy obtained with the DFT values of exchange, DMI, and MAE are given in Table II. The DW widths obtained for Co/Ir(111)
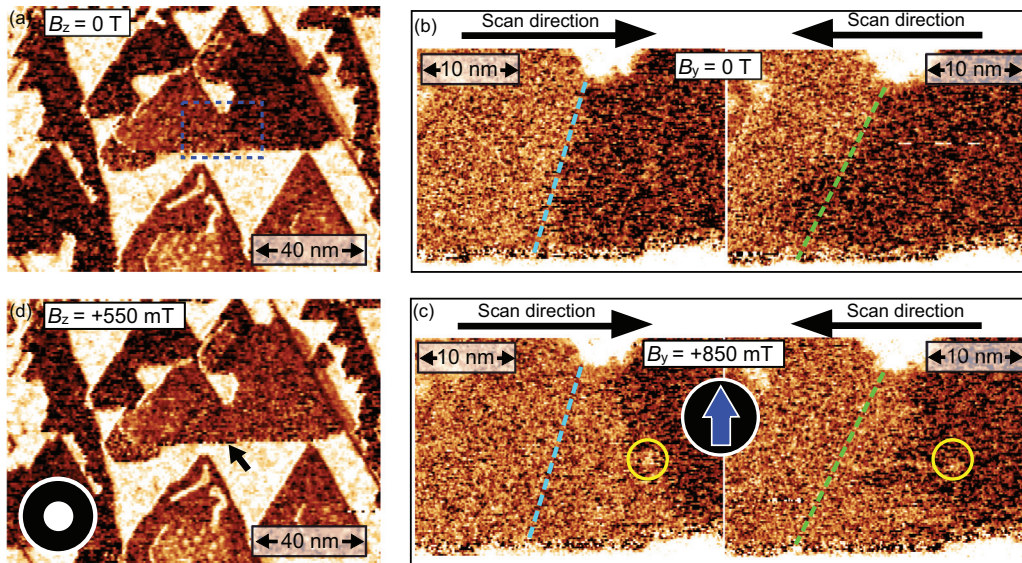

FIG. 6. (a)–(d) Spin-resolved dI/dU maps of Co ML islands with out-of-plane magnetic sensitivity. (a) The DW occurs at the coalescence point of two Co islands. The dotted blue rectangle indicates the area imaged in (b) and (c) in zero field and with an in-plane field in the y direction, respectively. The direction of the magnetic field is indicated by the blue arrow. The dashed lines mark the position of the wall in the forward (left) and backward (right) scans at zero field. In both cases the wall tilts in an in-plane field with respect to these lines. The yellow circle indicates an impurity in the Co, possibly acting as a pinning center for the wall. (d) Same area as in (a), imaged while applying an upward-pointing out-of-plane magnetic field. The expanding bright domain indicates that it points along the field direction. In all measurements $U = -450$ mV, $I = 350$ pA, $T = 4.7$ K.
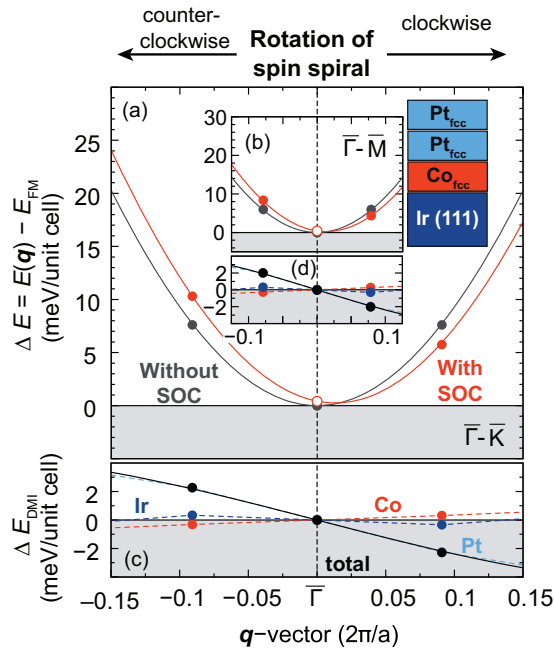
FIG. 7. (a) and (b) Calculated energy dispersion $E(\mathbf{q})$ of flat, cycloidal spin spirals for Pt/Pt/Co/Ir(111) without (gray dots) and with (red dots) spin-orbit interaction for left- and rightrotating spin spiral states in the $\overline{\Gamma}$-$\overline{K}$ and $\overline{\Gamma}$-$\overline{M}$ directions, respectively. The gray line is a fit of the dispersion to the Heisenberg model; the red line is a fit including the DMI and the magnetocrystalline anisotropy. (c) and (d) Element-resolved energy contribution for Pt/Pt/Co/Ir(111) due to Dzyaloshinskii-Moriya interaction $\Delta E_{DMI}(\mathbf{q})$. Note that the total DMI is the sum of all contributions. The black curve is the fit of the DMI. All fits are made within the nearest-neighbor approximation.

and Pt/Co/Ir(111) are in good agreement with the experimental values. Consistent with the spin spiral energy dispersions and the experimental observations, DWs are energetically unfavorable ($\Delta E_{DW-FM} > 0$) for Co/Ir(111) and Pt/Co/Ir(111). The smaller DW energy in Pt/Co/Ir(111) seems to disagree with the experimental observation of DWs being more likely to occur on the Co ML. However, the difference between the two DW energies is small with respect to the accuracy of the parameters. An error of only 0.1 meV in the value of either K or D can lead to ΔE_{DW-FM} values which are energetically degenerate. Due to the high sensitivity of ΔE_{DW-FM} to the magnetic parameters, it is not possible to predict where the DWs will occur more often.

IV. CONCLUSION

We have combined SP-STM measurements and DFT calculations to investigate DWs and interfacial DMI in pseudomorphic Co/Ir(111) and Pt/Co/Ir(111) ultrathin films. We observed DMI-stabilized Néel walls with a fixed rotational sense, separating out-of-plane magnetic domains. Our calculations showed a clockwise sense of magnetization rotation across the walls, in agreement with what has been observed in Ref. [22]. The calculated DMI increases by more than a factor of 2 in the sandwich structure. However, this increase is dominated by Pt with a negligible Ir contribution. For a Co double layer between Pt and Ir, on the other hand, both interfaces contribute

significantly to the total DMI. This highlights the importance of interlayer hybridization and Co film thickness in determining the total value of the DMI in magnetic multilayers.

APPENDIX A: DETERMINATION OF THE ABSOLUTE DOMAIN WALL ROTATIONAL SENSE USING DOMAIN WALL TILTING

In ultrathin magnetic films a sufficiently large DMI can stabilize Néel-type noncollinear structures, such as the DWs observed in Figs. 1 and 2. The spins in such walls are in a cycloidal configuration, where their plane of rotation is perpendicular to the wall itself. The absolute rotational sense of a Néel DW can be determined by observing its changes upon the application of an in-plane magnetic field along the wall [46]. To illustrate this, we have performed spin dynamics simulations of two DWs with opposite rotational sense in in-plane magnetic fields.

We consider the following Hamiltonian:

$$\mathcal{H} = -J \sum_{<ij>} (\mathbf{m_i} \cdot \mathbf{m_j}) - \mathbf{D} \sum_{<ij>} (\mathbf{m_i} \times \mathbf{m_j}) \\ + K \sum_i \left(m_i^z \right)^2 - \sum_i \mu_S \mathbf{B} \cdot \mathbf{m_i}, \quad (A1)$$

where $\mathbf{m_i} = \frac{\mathbf{M_i}}{M_i}$ is the unit vector of the magnetic moment at atom site i. We consider the exchange interaction and the DMI as acting only between nearest neighbors, with strength J and $\mathbf{D}$, respectively. K represents the uniaxial magnetocrystalline anisotropy, and the last term accounts for the Zeeman energy due to an external magnetic field $\mathbf{B}$. The values of J, $|\mathbf{D}|$, and K are the ones calculated by DFT and shown in Table I in the main text for the Co/Ir(111) case. We use a magnetic moment of $\mu_S = 2.2 \, \mu_B$ per atom, which is the sum of the calculated moment of the Co atoms (1.9 μ_B) and the induced moment of the interface Ir atoms (0.3 μ_B). We solve the Landau-Lifshitz-Gilbert equation [47,48] using a semi-implicit method [49] for DWs stabilized by opposite directions of $\mathbf{D}$. Figures 5(a) and 5(b) show the equilibrium configurations without magnetic field; Figs. 5(c) and 5(d) show those upon application of a magnetic field in the in-plane (here, y) direction. The field tilts the spins of the wall toward the field direction, but since the Néel configuration is favored by the DMI, the DW also tilts to partially recover the cycloidal state. For a clockwise (counterclockwise) rotation preferred by the DMI, the wall tilts in the positive (negative) direction according to our notation.

Thus we can experimentally determine the rotational sense of the DWs on Co/Ir(111) from the direction of the DW tilting in an in-plane magnetic field. We select a DW [see Fig. 6(a)] and image it in the absence of a magnetic field

to determine its position [see Fig. 6(b)]. The DW is in slightly different positions when scanning in the forward and backward directions, indicated by the dashed lines in Fig. 6(b). Such a difference can occur when the tip has a small residual stray field. This may drag the wall back and forth during scanning. We then apply the magnetic field along the y direction, as indicated by the blue arrow in Fig. 6(c), and observe a tilting in both forward and backward scans. From the direction of the tilting we deduce the direction of the in-plane magnetization of the wall to be pointing to the right. To determine the absolute rotational sense, it is necessary to assign the out-of-plane magnetization directions of the adjacent domains. This is done by applying a magnetic field in the out-of-plane direction.

This is visible in Fig. 6(d), where the bright domain, indicated by the black arrow, has expanded, while the dark one has shrunk. The bright (dark) areas in the Co correspond then to the domains pointing upward (downward), and therefore the magnetization across the wall rotates clockwise, as in Figs. 5(a) and 5(c) and in agreement with DFT calculations presented in the main text. The observed tilting angle is larger than the one expected from Fig. 5, possibly because the wall is attracted to an impurity [see yellow circles in Figs. 6(b) and 6(c)] which acts as a pinning center, although the DW still

tilts in the direction favored by the DMI. In the absence of impurities and with a noninteracting tip, this method allows us to quantify the strength of the DMI in the system. This can be done by measuring the tilting angle as a function of the applied in-plane magnetic field and then finding the correct value of D to reproduce such tilting in a spin dynamics simulation based on reasonable assumptions for J and K.

APPENDIX B: SPIN SPIRAL ENERGY DISPERSION OF PT/PT/CO/IR(111)

We have also performed calculations for a double layer of fcc Pt on Co/Ir(111), i.e., Pt/Pt/Co/Ir(111). The parameters for the structural relaxation can be found in Table I, and the spin spiral calculations, which are performed in the same way as the ones in the main text, are presented in Fig. 7. Adding a second layer of Pt to Pt/Co/Ir(111) gives rise to a DMI strength similar to that in Pt/Co/Ir(111) (see Fig. 4 of the main text), but the total DMI [Figs. 7(c) and 7(d)] is mostly due to Pt, while Ir has an even smaller contribution than in Pt/Co/Ir(111). The negligible Ir contribution to the DMI, caused by the addition of a Pt layer on top of the Co, is therefore not significantly affected by the number of Pt top layers.

[1] S. S. P. Parkin, M. Hayashi, and L. Thomas, Science **320**, 190 (2008).

[2] A. Fert, V. Cros, and J. Sampaio, Nat. Nanotechnol. **8**, 152 (2013).

[3] C. Moreau-Luchaire, C. Moutafis, N. Reyren, J. Sampaio, C. A. F. Vaz, N. Van Horne, K. Bouzehouane, K. Garcia, C. Deranlot, P. Warnicke, P. Wohlhüter, J.-M. George, M. Weigand, J. Raabe, V. Cros, and A. Fert, Nat. Nanotechnol. **11**, 444 (2016).

[4] O. Boulle, J. Vogel, H. Yang, S. Pizzini, D. de Souza Chaves, A. Locatelli, T. O. Menteş, A. Sala, L. D. Buda-Prejbeanu, O. Klein, M. Belmeguenai, Y. Roussigné, A. Stashkevich, S. M. Chérif, L. Aballe, M. Foerster, M. Chshiev, S. Auffret, I. M. Miron, and G. Gaudin, Nat. Nanotechnol. **11**, 449 (2016).

[5] J. F. Pulecio, A. Hrabec, K. Zeissler, R. M. White, Y. Zhu, and C. H. Marrows, arXiv:1611.06869.

[6] A. Soumyanarayanan, M. Raju, A. L. Gonzalez Oyarce, A. K. C. Tan, M.-Y. Im, A. P. Petrović, P. Ho, K. H. Khoo, M. Tran, C. K. Gan, F. Ernult, and C. Panagopoulos, Nat. Mater. **16**, 898 (2017).

[7] S. Heinze, K. von Bergmann, M. Menzel, J. Brede, A. Kubetzka, R. Wiesendanger, G. Bihlmayer, and S. Blügel, Nat. Phys. **7**, 713 (2011).

[8] A. Bogdanov and D. A. Yablonskii, Sov. Phys. JETP **68**, 101 (1989).

[9] A. N. Bogdanov and U. K. Rößler, Phys. Rev. Lett. **87**, 037203 (2001).

[10] I. E. Dzyaloshinskii, J. Phys Chem. Solids **4**, 241 (1958).

[11] T. Moriya, Phys. Rev. Lett. **4**, 228 (1960).

[12] A. Crépieux and C. Lacroix, J. Magn. Magn. Mater. **182**, 341 (1998).

[13] M. Bode, M. Heide, K. von Bergmann, P. Ferriani, S. Heinze, G. Bihlmayer, A. Kubetzka, O. Pietzsch, S. Blügel, and R. Wiesendanger, Nature (London) **447**, 190 (2007).

[14] M. Heide, G. Bihlmayer, and S. Blügel, Phys. Rev. B **78**, 140403 (2008).

[15] A. Thiaville, S. Rohart, É. Jué, V. Cros, and A. Fert, Europhys. Lett. **100**, 57002 (2012).

[16] N. Romming, C. Hanneken, M. Menzel, J. E. Bickel, B. Wolter, K. von Bergmann, A. Kubetzka, and R. Wiesendanger, Science **341**, 636 (2013).

[17] A. R. Fert, Mater. Sci. Forum **59-60**, 439 (1990).

[18] A. W. J. Wells, P. M. Shepley, C. H. Marrows, and T. A. Moore, Phys. Rev. B **95**, 054428 (2017).

[19] B. Dupé, G. Bihlmayer, M. Böttcher, S. Blügel, and S. Heinze, Nat. Commun. **7**, 11779 (2016).

[20] B. Dupé, M. Hoffmann, C. Paillard, and S. Heinze, Nat. Commun. **5**, 4030 (2014).

[21] H. Yang, A. Thiaville, S. Rohart, A. Fert, and M. Chshiev, Phys. Rev. Lett. **115**, 267210 (2015).

[22] G. J. Vida, E. Simon, L. Rózsa, K. Palotás, and L. Szunyogh, Phys. Rev. B **94**, 214422 (2016).

[23] H. Yang, O. Boulle, V. Cros, A. Fert, and M. Chshiev, arXiv:1603.01847.

[24] G. Chen, A. T. N'Diaye, Y. Wu, and A. K. Schmid, Appl. Phys. Lett. **106**, 062402 (2015).

[25] E. C. Corredor, S. Kuhrau, F. Kloodt-Twesten, R. Frömter, and H. P. Oepen, Phys. Rev. B **96**, 060410 (2017).

[26] S. Meckler, N. Mikuszeit, A. Preßler, E. Y. Vedmedenko, O. Pietzsch, and R. Wiesendanger, Phys. Rev. Lett. **103**, 157201 (2009).

[27] A. Hrabec, N. A. Porter, A. Wells, M. J. Benitez, G. Burnell, S. McVitie, D. McGrouther, T. A. Moore, and C. H. Marrows, Phys. Rev. B **90**, 020402 (2014).

[28] J. E. Bickel, F. Meier, J. Brede, A. Kubetzka, K. von Bergmann, and R. Wiesendanger, Phys. Rev. B **84**, 054454 (2011).

[29] O. Pietzsch, A. Kubetzka, D. Haude, M. Bode, and R. Wiesendanger, Rev. Sci. Instrum. **71**, 424 (2000).

[30] S. Meckler, M. Gyamfi, O. Pietzsch, and R. Wiesendanger, Rev. Sci. Instrum. **80**, 023708 (2009).

[31] E. Wimmer, H. Krakauer, M. Weinert, and A. J. Freeman, Phys. Rev. B **24**, 864 (1981).

[32] H. J. F. Jansen and A. J. Freeman, Phys. Rev. B **30**, 561 (1984).

[33] H. Krakauer, M. Posternak, and A. J. Freeman, Phys. Rev. B **19**, 1706 (1979).

[34] FLEUR, www.flapw.de.

[35] S. H. Vosko, L. Wilk, and M. Nusair, Can. J. Phys. **58**, 1200 (1980).

[36] Y. Zhang and W. Yang, Phys. Rev. Lett. **80**, 890 (1998).

[37] P. Kurz, F. Förster, L. Nordström, G. Bihlmayer, and S. Blügel, Phys. Rev. B **69**, 024415 (2004).

[38] B. Zimmermann, M. Heide, G. Bihlmayer, and S. Blügel, Phys. Rev. B **90**, 115427 (2014).

[39] L. M. Sandratskii, J. Phys.: Condens. Matter **3**, 8565 (1991).

[40] M. Heide, G. Bihlmayer, and S. Blügel, Phys. B **404**, 2678 (2009).

[41] S. Meyer, B. Dupé, P. Ferriani, and S. Heinze, Phys. Rev. B **96**, 094408 (2017).

[42] A. Oswald, R. Zeller, P. J. Braspenning, and P. H. Dederichs, J. Phys. F **15**, 193 (1985).

[43] A. Liechtenstein, M. Katsnelson, V. Antropov, and V. Gubanov, J. Magn. Magn. Mater. **67**, 65 (1987).

[44] K. von Bergmann, A. Kubetzka, O. Pietzsch, and R. Wiesendanger, J. Phys.: Condens. Matter **26**, 394002 (2014).

[45] P. Bruno, Phys. Rev. Lett. **83**, 2425 (1999).

[46] O. Boulle, S. Rohart, L. D. Buda-Prejbeanu, E. Jué, I. M. Miron, S. Pizzini, J. Vogel, G. Gaudin, and A. Thiaville, Phys. Rev. Lett. **111**, 217203 (2013).

[47] L. Landau and E. Lifshitz, Phys. Zeitsch. der Sow. **8**, 153 (1935).

[48] T. L. Gilbert, IEEE Trans. Magn. **40**, 3443 (2004).

[49] J. Mentink, M. Tretyakov, A. Fasolino, M. Katsnelson, and T. Rasing, J. Phys.: Condens. Matter **22**, 176001 (2010).